Effect of environmental ageing on the numerical response of FRP-strengthened masonry walls

Bahman Ghiassi[1], Paulo B. Lourenço[2] Daniel V. Oliveira[3]

ISISE, University of Minho, Department of Civil Engineering, Guimarães, Portugal

ABSTRACT

Recent durability studies have shown the susceptibility of bond in FRP-masonry components to hygrothermal exposures. However, it is not clear how this local material degradation affects the global behavior of FRP-strengthened masonry structures. This study addresses this issue by numerically investigating the nonlinear behavior of FRP-masonry walls after ageing in two different environmental conditions.

A numerical modeling strategy is adopted and validated with existing experimental tests on FRP-strengthened masonry panels. The model, once validated, is used for modeling of four hypothetical FRP-strengthened masonry walls with different boundary conditions, strengthening schemes and reinforcement ratios. The nonlinear behavior of the walls is then simulated before and after ageing in two different environmental conditions. The degradation data are taken from previous accelerated ageing tests performed by the authors. The changes in the failure mode and nonlinear response of the walls after ageing are presented and discussed.

Keywords: FRP; masonry; durability; numerical modeling; long-term performance.

[1]Postdoctoral researcher, ISISE, University of Minho, Department of Civil Engineering, Azurém, 4800-058 Guimarães, Portugal. Phone: +351 253 510 499, fax: +351 253 510 217, E-mail: bahmanghiassi@civil.uminho.pt

[2] Professor, ISISE, University of Minho, Department of Civil Engineering, Azurém, 4800-058 Guimarães, Portugal. Phone: +351 253 510 209, fax: +351 253 510 217, E-mail: pbl@civil.uminho.pt

[3]Associate Professor, ISISE, University of Minho, Department of Civil Engineering, Azurém, 4800-058 Guimarães, Portugal. Phone: +351 253 510 247, fax: +351 253 510 217, E-mail: danvco@civil.uminho.pt

Introduction

There has been an extensive effort in the last decades for developing suitable strengthening techniques for application to masonry structures. Fiber Reinforced Polymers (FRPs) have been increasingly used for externally bonding to masonry walls. Several experimental studies have been carried out on the effectiveness of this strengthening technique, see e.g. (Karantoni and Fardis 1992; Valluzzi et al. 2002; Tumialan et al. 2003; Milani et al. 2006; Mosallam and Banerjee 2011). Few numerical models have also been developed for simulating the complex nonlinear behavior of FRP-strengthened masonry elements, see e.g. (Milani and Lourenço 2013; Grande et al. 2013). The available information shows that this strengthening technique suitably improves the structural performance of unreinforced masonry.

The efficacy and reliability of the external strengthening techniques are intrinsically dependent on the bond between the composite material and the substrate. The bond behavior has been extensively studied in FRP-concrete systems, but it has only recently received attention in case of FRP-masonry (Garbin et al. 2010; Ghiassi et al. 2012; Carrara et al. 2013). Meanwhile, the durability and long-term performance of bond remains a challenge for both FRP bonded masonry and concrete components.

Structures are exposed to environmental changes or degrading agents, such as temperature and moisture variations or alkaline agents, during their service life. These changes can affect the materials behavior and performance of the structure to a large extent, which should be considered at the design stage or should be foiled with innovative solutions. Few studies can be found in the literature in which the durability of bond in FRP-masonry components has been investigated by performing accelerated ageing tests (Sciolti et al. 2012; Ghiassi et al 2013; Ghiassi et al. 2014a; Ghiassi et al. 2014b). The experimental results show that environmental conditions, especially in case of high relative humidity levels, can cause severe degradation in the bond performance and therefore can threat the effectiveness of the applied strengthening. While, a better understanding of the degradation mechanisms requires performing more comprehensive experimental tests, the effect of local material and bond degradation on the structural performance is also not clear. This paper addresses the latter issue by numerically investigating the nonlinear behavior of FRP-strengthened masonry walls before and after environmental ageing.

Researchers have used different approaches for modeling FRP-masonry systems including: assuming a perfect bond between FRP and masonry substrate (Ascione et al. 2005; Grande et al. 2013); using interface elements for modeling the bond behavior between FRP and masonry (Failla et al. 2005; Ghiassi et al. 2012); or using homogenization techniques (Milani and Lourenço 2013). As the bond behavior is the main mechanism affected by the environmental exposures in this strengthening technique (Ghiassi et al. 2014a), using interface elements to represent its behavior and degradation seems a more suitable approach in durability studies and therefore is used here.

A two-dimensional nonlinear Finite Element (FE) model is adopted for modeling the behavior of FRP-strengthened masonry walls subjected to in-plane loading conditions. The numerical model is initially validated by simulating some reference experimental tests on strengthened masonry panels taken from literature (Milani et al. 2006). Four hypothetical masonry walls with different strengthening schemes and FRP widths are then selected to address the main objectives of this study. The changes in the nonlinear behavior and failure mode of the walls after ageing in two different environmental conditions are investigated and the results are presented and discussed.

The material and bond degradation data are taken from accelerated ageing tests performed and reported in (Ghiassi et al. 2014a).

A brief review of durability tests

A comprehensive experimental program was carried out at the University of Minho to investigate the hygrothermal degradation of bond in FRP-strengthened masonry units by performing accelerated ageing tests, see (Ghiassi et al 2014a) for detailed information. A brief review of the experimental tests and observations is given in this section.

The tests included exposing GFRP-strengthened brick specimens, see Fig. 1(a), to accelerated hygrothermal conditions in a climatic chamber. Suitable specimens from material constituents (brick cubes, epoxy dog-bone shape specimens and GFRP coupons), see Fig. 1(b), were also exposed to the same environmental conditions to investigate the changes in their mechanical properties. Mechanical characterization tests were performed on the specimens after different exposure periods to investigate the degradation in the material properties and the bond between GFRP and brick substrate.

The GFRP-strengthened brick specimens were prepared following the wet layup procedure according to the geometrical details shown in Fig. 1(a). Solid clay bricks with dimensions of 200x100x50 mm^3 and GFRP composites were used as the substrate and strengthening material, respectively.

After curing, the specimens were exposed to accelerated environmental conditions. The hygrothermal exposures consisted of 6 hours temperature cycles from +10℃ to +50℃ and constant relative humidity of 90% (called exposure HT1) and 60% (called exposure HT2), see Fig. 2(a). The specimens were subjected to a total of 225 cycles of HT1 and 820 cycles of HT2 conditions. Five specimens, of each test type, were periodically taken from the climatic chamber for exploring the possible changes in the material and bond mechanical properties, see Fig. 2(b, c).

Material characterization tests included compressive tests on brick cubes and tensile tests on epoxy resin and GFRP coupons according to applicable test standards. The bond behavior was characterized by performing single-lap shear bond tests.

Visual inspection and IR thermography tests on the exposed specimens showed that a progressive FRP delamination was occurring with time increment (Ghiassi et al. 2014b). The delaminations, being at the FRP/brick interface, were larger in the specimens subjected to HT1 cycles. Mechanical tests showed negligible degradation in the compressive strength of the bricks. However, some degradation occurred in the tensile strength of epoxy resin, GFRP coupons and bond strength. The changes in the material and bond properties are normalized to the un-aged condition and are presented in Fig. 3. The decay models obtained from a regression analysis on the experimental data are also presented in this figure with a solid line.

It seems that the degradation in the specimens exposed to HT2 conditions has reached a residual value. However, this conclusion cannot be made for the specimens exposed to HT1 conditions and further tests with longer exposure times are necessary. The observed degradation is higher in the specimens exposed to HT1 conditions due to the existence of a high level of relative humidity.

Modeling FRP-masonry walls

The adopted strategy for modeling the nonlinear behavior of FRP-strengthened masonry walls is presented in this section. The accuracy of the adopted model is verified by comparing the numerical results with experimental tests taken from literature.

Outline

A two-dimensional nonlinear Finite Element (FE) model is adopted for modeling the behavior of the FRP-strengthened masonry walls. For the masonry, a macro-modeling strategy is followed using a softening anisotropic elasto-plastic continuum model (Lourenço 1998). The FRP strips, assumed to have linear elastic behavior, are attached to the masonry surface with interface elements. The interface elements are introduced with a suitable bond-slip law.

The analysis is carried out in the FE code DIANA (2014). The adopted meshes include eight-node (denoted by CQ16M) and 6-node plane stress elements (denoted by CT12M) to model the masonry panel. The FRP strips are modeled, in a simplified way, with truss elements (denoted by LT2RU), and 6-node zero-thickness interface elements (denoted as CL12I) are used for the interface elements.

The nonlinear analysis is performed by incremental application of the load (or displacement) until failure. The arc-length method, combined with the linear stiffness iteration method and an energy norm criterion, are adopted to solve the resulting system of non-linear equations.

Material models

The softening anisotropic elasto-plastic continuum model used for modeling the masonry behavior is based on the studies of Lourenço (1998). This model consists of an extension of conventional theories for quasi-brittle materials to describe the orthotropic behavior. A Hill-type yield criterion in compression and a Rankine-type yield criterion in tension are used as yield functions. The nonlinear behavior in compression is characterized by parabolic hardening followed by parabolic/exponential softening, while exponential softening is used for tension. A detailed explanation of the material model and its theoretical background can be found in (Lourenço 1998). Three factors termed α, β and γ are required for this material model, which are taken equal to 1.73, –1.05 and 1.2 as suggested in (Grande et al. 2008). Here, α accounts for shear stress contribution in tensile failure, β couples the normal compressive stresses and γ considers the shear stress contribution in compressive failure. The equivalent plastic strain corresponding to the peak compressive stress is taken as 0.0008 (Grande et al. 2008).

An isotropic elastic material model is used for FRP strips. For the interface elements, the trilinear bond-slip law proposed in (Ghiassi et al. 2012) is adopted and calibrated according to the reference experimental tests.

Validation of the numerical model

The accuracy of the adopted macro-modeling approach is assessed in this section by comparing the numerical results with some available experimental tests. The tests performed by Milani et al. (2006) are chosen as reference tests to serve as a basis for numerical validation.

The tests are performed on small-scale masonry panels strengthened with CFRP strips to study the effectiveness of externally bonded reinforcement on the in-plane response of masonry walls. The specimens consisted of 9 panels of 290×270 mm^2 (L×H) named Pan A, Pan B and Pan C, and 3 panels of 416×414 mm^2 (L×H) named PanWin A and Pan Win B with a central opening with dimensions of 184×156 mm^2. The panels were built of small clay bricks with dimensions of

56×15 mm^2 and cement-lime mortar joints. The thickness of the walls was equal to 30 mm. Panels Pan A, Pan B and Pan C were placed on two steel plates with length of 40 mm disposed at the lower edge corners and positioned on steel rollers to allow rotation of the supports. Series PanWin A and PanWin B were placed on two steel plates positioned directly on a stiff beam, limiting the rotation of the supports in this case.

Panels Pan A (bare masonry wall) and Pan C (strengthened panel with diagonal strips) are selected here for verification of the numerical model, see Fig. 4. In Pan C, the reinforcement consists of CFRP strips with 12.5 mm width and 0.2 mm thickness applied on both sides of the wall. The elastic modulus of FRP strips was 160 GPa.

The panels were loaded vertically with the aid of a steel plate with dimensions of 70×30 mm^2. The loads were applied by means of a 100 kN jack and the displacements were measured with two LVDTs placed on top of the walls, next to the load cell (on the steel plate used for load application). The mechanical parameters of masonry panels, obtained based on experimental results and theoretical considerations and also used for numerical modeling in (Milani et al. 2006; Grande et al. 2008), are presented in Table 1. Here, x is the bed joint direction and y is the head joint direction. The trilinear bond-slip law proposed in (Ghiassi et al. 2012) is adopted and calibrated according to the reference experimental tests for the interface elements, see Table 2.

Regarding the observed failure mode, Pan A (bare masonry panel) failed due to cracking of masonry showing vertical tensile cracks followed by a relatively ductile behavior. In case of Pan C (the strengthened panel), vertical and diagonal cracks were observed in the masonry panel combined with delamination of FRP strips at the lower extremes.

In the numerical model, the boundary conditions are applied as given in the reference experimental tests. A monotonic incremental load is applied on top of the wall according to the experimental test setup. A schematic view of the adopted FE mesh is shown in Fig. 5(a). The numerical force-displacement curves of both panels are shown in Fig. 5(b) together with the experimental results. It can be observed that a good agreement is found between the numerical and experimental results for both un-strengthened (Pan A) and strengthened (Pan C) panels. The developed plastic strains in the panels at the peak load level are also shown in Fig. 6. Similar to experimental results, Pan A has flexural cracks at the bottom while vertical cracks occurred in Pan C at higher load levels with FRP delamination at the bottom. Here, it is noted that a non-symmetric configuration is obtained (only) at failure due to the fact that the FE mesh is also not symmetric, meaning that localization occurs in one side (as also obtained in the tests).

The results show the accuracy of the adopted strategy in the numerical modeling. Numerical modeling is therefore used in the next section to investigate the effect of local bond degradation on the global performance of FRP-strengthened masonry walls.

Effect of degradation on the structural response

Four hypothetical FRP-strengthened panels with different strengthening schemes and ratio, and different boundary conditions are selected in this section. The aim is to investigate the effect of materials and bond degradation on the global response of the strengthened walls. The modeling strategy, element types and material models are the same as explained in sec. 3.

The selected walls have the same dimensions as reference panels (290×270 mm^2). Three common strengthening schemes are chosen as shown in Fig. 7. GFRP composites with equivalent thickness of 0.48 mm, elastic modulus of 80 GPa and tensile strength of 1250 MPa (as obtained experimentally) are used as the strengthening material. GFRP is selected due to the fact that the experimental degradation data is for this material.

The walls are analyzed under later loading with two different boundary conditions of fixed (bottom)-free (top) and fixed-fixed. The latter boundary condition is expected to provide diagonal tension cracking while the former is expected to provide rocking behavior in the walls. Different FRP widths of 6 mm, 12.5 mm and 25 mm are assumed for strengthening to investigate the effect of FRP axial stiffness and reinforcement ratio. The analysis is performed by application of incremental lateral displacements until failure. A summary of the selected walls is presented in Table 3.

The framework followed is presented in Fig. 8. The panels are first analyzed without considering any degradation to obtain the un-aged nonlinear response. The analysis is then repeated with the degraded material properties including the bond (corresponding to interface elements) and GFRP mechanical properties. The degradation data are taken from accelerated ageing results (presented in sec. 2) at 225 cycles of HT1 (temperature cycles of +10°C to +50°C with 90% constant relative humidity) and HT2 (temperature cycles of +10°C to +50°C with 60% constant relative humidity) exposures, see Table 4. The exposure time of 225 cycles is selected at the end of exposure HT1 to avoid extrapolation of the degradation data. Since no degradation was observed in the mechanical properties of the bricks, the masonry mechanical properties are assumed to be intact after ageing.

The experimental results showed that FRP delamination length was on average 30% of the bonded length after 225 cycles of HT1 exposure, while this value was less than 10% in HT2 exposure (Ghiassi et al. 2014b). The effect of environmental induced FRP delamination is also investigated here (only in models with $FRP_w = 6$ mm and exposed to HT1 conditions) by reducing the length of FRP by 30% as was observed in the experiments. Since the FRP delamination in the specimens exposed to HT2 condition was small, it has not been considered in this study. The delamination is considered to occur at both FRP ends (called with suffix –PD hereafter) or only at the top end (called with suffix –PD2 hereafter).

A simple degradation model is assumed for the bond-slip law to consider the bond environmental degradation, see Fig. 9. Based on this model, the bond strength and stiffness decrease according to the degradation in the bond fracture energy, while the other parameters remain constant. The changes in the bond-slip law parameters due to environmental exposures are therefore obtained and presented in Table 5.

Behavior of un-aged walls

The numerical load-displacement curves of the walls before and after strengthening with different FRP widths are shown in Fig. 10.

Wall 1 has a rocking failure mode before strengthening as it was expected from the boundary and loading conditions. Application of GFRP sheets according to strengthening scheme 1 changes the failure mode to diagonal tension cracking, see Fig. 11(b). The distribution of tensile plastic strains shows that a compressive strut is formed between the two vertical FRP sheets in the strengthened walls. The load-displacement curves show that the lateral strength of the wall increase with the FRP width, while the stiffness remains high for a larger part of the response. The analysis is continued until compressive crushing of the masonry strut, leading to convergence of all the force-displacement curves corresponding to walls with different strengthening ratio.

Application of diagonal strengthening, Wall 2, resulted in a large increment of the wall lateral strength without changing the failure mode, see Fig. 10(b), while again the stiffness remains high for a larger branch. In the wall with FRP_w=6 mm, tensile rupture of the FRP has occurred in the last step and the analysis is stopped upon this moment. The tensile plastic strain distribution on the masonry wall corresponding to the peak load is presented in Fig. 11(c). In the walls with FRP_w=12.5 mm and FRP_w=25 mm, the rocking movement continues until the masonry toe compression. It seems that the effect of FRP width in these walls is insignificant in increasing the wall lateral strength, although cracking is better controlled and higher stiffness is obtained in the inelastic phase.

Wall 3 has a different boundary condition (restrained vertical displacements at top) and therefore the bare wall failed in diagonal tension cracking with a lateral strength higher than Wall 1 and Wall 2, see also Fig. 12(a). Application of FRP strengthening resulted in significant increment of the wall lateral strength and post-cracking stiffness until FRP tensile rupture, see Fig. 10(c). The tensile plastic strain distribution on the masonry wall corresponding to the peak load is shown in Fig. 12(b).

Wall 4 has the same boundary condition as Wall 3 but is strengthened with horizontal FRP sheets, see Fig. 7(c). The lateral strength of the will is increased after strengthening. The effect of FRP width on the global behavior seems insignificant showing low exploitation of FRP in this strengthening scheme, see Fig. 10(d). The walls fail in diagonal tension cracking after strengthening, with the compressive strut formed between two horizontal FRP sheets, see Fig. 12(c).

Behavior of walls after ageing

The summary of the analysis results is presented in Table 6 and Table 7 in terms of the changes in the peak strength and failure mode of the walls after ageing. The force-displacement curves of the walls with 6 mm FRP width are also shown in Fig. 13. Exposure HT2 did not induce significant changes in the force-displacement response of the walls (besides reduction of the peak strength) and therefore these curves are not presented.

In general, the walls exposed to HT1 conditions, representing environments with high relative humidity, have higher reduction of lateral strength. Exposure HT2, representing environments with average relative humidity, has induced maximum degradation of 12.4%, in Wall 3 with FRP_w=25 mm. The reduction of lateral strength in other walls after ageing in HT2 condition is negligible. HT1 condition (without considering FRP delamination) has induced maximum reduction of 19%, in Wall 2 with FRP_w=6 mm. Significant reduction of wall strength and change of failure mode is observed when FRP delamination is considered together with the bond and material degradation.

The effect of material degradation in the walls lateral strength decreases with increment of FRP width with an exception in Wall 3. This can be explained with the FRP exploitation level in different strengthening conditions. Fig. 14 shows the developed axial stress in the FRP sheets at the peak load for the walls with FRP_w=6 mm and FRP_w=25 mm. It can be observed that ageing at HT1 condition has generally resulted in an increase in the maximum stress developed in FRP sheets. Moreover, it can be observed that increment of FRP width in Walls 1, 2 and 4 has resulted in lower exploitation of FRP composite and therefore decreasing the effect of local materials ageing at the global response. On the other hand, all the FRP tensile strength is exploited in wall 3 independently of the FRP width.

It can be observed that in Wall 1 with FRP_w=6 mm, FRP delamination at both sides (HT1-PD) has resulted in a change of failure mode from diagonal tension cracking to rocking at the bottom, see Fig. 15. The strength of the wall has also decreased significantly (67.9%) as the FRP does not contribute in the load resistance and the wall performs as a bare masonry. When the delamination was only considered at the top (HT1-PD2), diagonal tension failure occurred in the wall resulting in less reduction of the lateral resistance (32.9%) in comparison to HT1-PD, see Fig. 15. It can be seen that the diagonal compression strut has been formed between the FRP ends in both cases of HT1 and HT1-PD2.

In Wall 2, both end delamination (HT1-PD) has a similar effect and has resulted in change of failure mode to wall rocking and 82.1% reduction in the wall lateral strength. On the other hand, one-side delamination (HT1-PD2) has resulted in 54.6% reduction of lateral strength and change of failure mode to sliding at the top of the wall, see Fig. 16. In Walls 3 and 4, FRP delamination induced reduction of lateral strength of 13.0% and 30.8%, respectively, but the failure mode has not changed after delamination and degradation.

Conclusions

The effect of local bond and material degradation on the global performance of strengthened masonry walls was numerically investigated in this paper. Four hypothetical GFRP-strengthened masonry walls with different strengthening details, reinforcement ratio and boundary conditions were considered for this purpose.

A two-dimensional FE model, with plane stress elements adopted for masonry and truss elements for FRP composite connected with interface elements to the masonry surface, was used for modeling FRP-strengthened masonry panels subjected to in-plane loading. The model was initially validated by comparing the numerical results with experimental results taken from literature. Subsequently, the walls were modeled and analyzed at both un-aged and aged conditions. For modeling the behavior of the walls after ageing, the degraded material properties and bond characteristics were taken from accelerated ageing tests previously performed by the authors. Ageing was considered in two different environments with high and average relative humidity conditions. The changes in the global performance of the strengthened panels after ageing were investigated in terms of force-displacement curves and failure modes.

Different degradation levels in the global performance of the walls were observed. The largest degradation level occurred in the walls reinforced with a diagonal scheme (Wall 2 and 3) after exposure to HT1 condition (temperature cycles of +10°C to +50°C with 90% constant relative humidity). In some cases a change of failure mode after degradation was found. A solution to this problem can be the protection of the bonded area from the humidity attack or the use of hydrophobic epoxy resins. FRP delaminations, when considered in the numerical model, induced significant reduction of wall lateral strength and change of failure mode, which should be carefully considered in the design procedures. A solution to this problem can be the use of mechanical anchorages to avoid FRP delamination at the restrained sections. Although, the FRP delaminations can still occur in the un-anchored areas, mechanical anchorage can help in keeping the structural integrity and exploitation of the FRP tensile capacity.

The results showed that FRP width affects the degradation level occurred in the walls. The level of degradation decreased with increment of FRP width in all the walls besides Wall 3. The strengthening and geometrical detail of Wall 3 resulted in fully exploitation of FRP materials under tensile stresses independently from the FRP width. This led to obtaining larger reduction in the wall lateral strength in the walls with larger FRP widths, in contrary to the other walls. It was also observed that the bond degradation resulted in development of larger tensile stresses in FRP in Walls 1, 2 and 4.

The present results are a first step towards investigating the effect of materials degradation on the global performance of strengthened masonry structures. Modeling other strengthened panels and structures with different geometrical and strengthening details within three-dimensional FE models is necessary for better understanding the key factors and for proposing a durability-based design framework. However, this requires sound prevision models on bond strength and more extensive results on bond durability.

Acknowledgements

The first author acknowledges the financial support of the Portuguese Science Foundation (Fundação de Ciência e Tecnologia, FCT), through grants SFRH/BD/80697/2011 and SFRH/BPD/92614/2013.

References

Ascione, L., Feo, L., and Fraternali, F. (2005). "Load carrying capacity of 2D FRP/strengthened masonry structures." *Compos. Part B: Eng.*, 36(8), 619–26.

Carrara, P., Ferretti, D., and Freddi, F. (2013). "Debonding behavior of ancient masonry elements strengthened with CFRP sheets." *Compos. Part B: Eng.*, 45(1), 800–10.

DIANA (2014). "Displacement analysis finite element software." V. 9.5, TNO Building Division, Delft, The Netherlands.

Failla, A., Cottone, A., and Gianbanco, G. (2005). "Numerical modeling of masonry structures reinforced by FRP plate/sheets." *Structural analysis of historical constructions*, Taylor & Francis, 857–66.

Garbin, E., Panizza, M., and Valluzzi, M. R. (2010). "Experimental Assessment of Bond Behaviour of Fibre-Reinforced Polymers on Brick Masonry." *Struct. Eng. Intern.* , 20(4), 392-99.

Ghiassi, B., Marcari, G., Oliveira, D.V., and Lourenço, P.B. (2012). "Numerical analysis of bond behavior between masonry bricks and composite materials." *Eng. Struc.*, 43, 210–20.

Ghiassi, B., Marcari, G., Oliveira, D.V, and Lourenço, P.B. (2013). "Water degrading effects on the bond behavior in FRP-strengthened masonry." *Compos. Part B: Eng.*, 54, 11–19.

Ghiassi, B., Oliveira, D.V., and Lourenço, P.B. (2014a). “Accelerated hygrothermal ageing of bond in FRP-masonry systems.” *ASCE J. Compos. Constr.* (Accepted for publication).

Ghiassi, B., Silva, S.M., Oliveira, D.V., Lourenço, P.B., and Bragança, L. (2014b). “FRP-to-Masonry Bond Durability Assessment with Infrared Thermography Method.” *J. Nondestruct. Eval.*, Doi: 10.1007/s10921-014-0238-8.

Grande, E., Milani, G., and Sacco, E. (2008). “Modelling and analysis of FRP-strengthened masonry panels.” *Eng. Struct.*, 30(7), 1842–60.

Grande, E., Imbimbo, M., and Sacco, E. (2013). “Finite element analysis of masonry panels strengthened with FRPs.” *Compos. Part B: Eng.*, 45(1), 1296–309.

Karantoni, F. and Fardis, M. (1992). ”Effectiveness of Seismic Strengthening Techniques for Masonry Buildings.” *J. Struct. Eng.*, 118(7), 1884–1902.

Lourenço, P.B. (1998). “Continuum Model for Masonry: Parameter estimation and validation.” *J. Struct. Eng.*, 124(6), 642–52.

Milani, G., Rotunno, T., Sacco, E., and Tralli, A. (2006). “Failure Load of Frp Strengthened Masonry Walls : Experimental Results and Numerical Models.” *Struct. Dyn. Health Monit.*, 2(1), 29–50.

Milani, G., and Lourenço, P. B. (2013). “Simple Homogenized Model for the Nonlinear Analysis of FRP-Strengthened Masonry Structures . I : Theory.” *J. Eng. Mech.*, 139(1), 59–76.

Mosallam, A., and Banerjee, S. (2011). “Enhancement in in-plane shear capacity of unreinforced masonry (URM) walls strengthened with fiber reinforced polymer composites.” *Compos. Part B: Eng.*, 42(6), 1657–70.

Sciolti, M. S., Aiello, M. A., and Frigione, M. (2012). “Influence of water on bond behavior between CFRP sheet and natural calcareous stones.” *Compos. Part B: Eng.*, 43(8), 3239–50.

Tumialan, J., Galati, N., and Nanni, A. (2003). ”Field Assessment of Unreinforced Masonry Walls Strengthened with Fiber Reinforced Polymer Laminates.” *J. Struct. Eng.*, 129(8), 1047–1056.

Valluzzi, M.R., Tinazzi, D., Modena, C. (2002). “Shear behavior of masonry panels strengthened by FRP laminates.” *Constr. Build. Mater.* 16(7), 409-16.

List of Tables

Table 1. Masonry mechanical parameters.

Table 2. Bond-slip law parameters.

Table 3. Selected hypothetical walls.

Table 4. Material degradation after 225 cycles of all exposures.

Table 5. Bond-slip parameters at 225 cycles of hygrothermal exposures.

Table 6. Changes in the strength and failure mode of Wall 1 and Wall 2 after ageing.

Table 7. Changes in the strength and failure mode of Wall 3 and Wall 4 after ageing.

List of Figures

Fig. 1.Geometrical details of (a) bond characterization specimens; (b) material characterization specimens.

Fig. 2. (a) Exposure cycles; (c) single-lap shear test setup; (d) tensile test setup.

Fig. 3. Experimentally obtained hygrothermal degradation: (a) epoxy resin in HT1 environment; (b) epoxy resin in HT2 environment; (c) GFRP in HT1 environment; (d) GFRP in HT2 environment; (e) debonding force; (f) bond fracture energy.

Fig. 4. Panels selected for verification of the numerical model: (a) Pan A; (b) Pan C.

Fig. 5. (a) Adopted FE mesh for the reference walls; (b) comparison between numerical and experimental force-displacement curves.

Fig. 6. Tensile plastic strains in: (a) Pan A; (b) Pan C.

Fig. 7. Selected strengthening schemes: (a) scheme 1; (b) scheme 2; (c) scheme 3.

Fig. 8. Procedure followed for analysis of the walls.

Fig. 9. Degradation model for the bond-slip law.

Fig. 10. Force-displacement behavior of selected hypothetical walls: (a) Wall 1; (b) Wall 2; (c) Wall 3; (d) Wall 4.

Fig. 11. Tensile plastic strain distribution on (a) Walls 1 and 2 before strengthening; (b) Wall 1 after strengthening with FRP_w=6 mm;. (c) Wall 2 after strengthening with FRP_w=6 mm

Fig. 12. Tensile plastic strain distribution on (a) Walls 3 and 4 before strengthening; (b) Wall 3 after strengthening with FRP_w=6 mm;. (c) Wall 4 after strengthening with FRP_w=6 mm.

Fig. 13. Force-displacement behavior of selected hypothetical walls after ageing: (a) Wall 1; (b) Wall 2; (c) Wall 3; (d) Wall 4.

Fig. 14. FRP axial stress distribution at the peak load in: (a) Wall 1; (b) Wall 2; (c) Wall 3; (d) Wall 4.

Fig. 15. Tensile plastic strain distribution on Wall 1 aged in different conditions.

Fig. 16. Tensile plastic strain distribution on Wall 2 aged in different conditions.

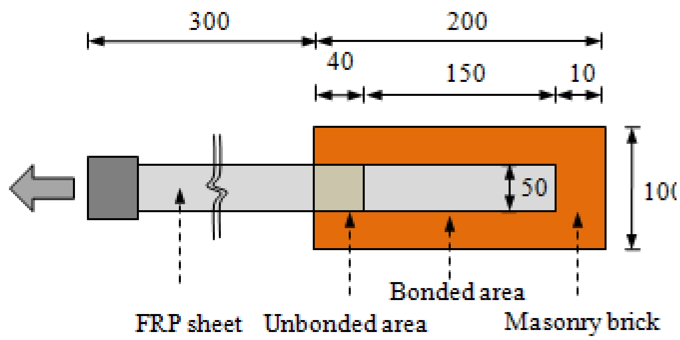

(a)

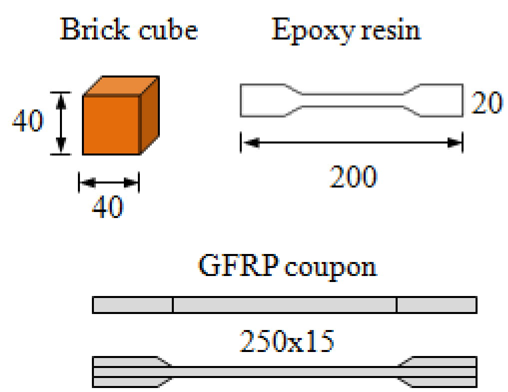

(b)

Fig. 1.Geometrical details of: (a) bond characterization specimens; (b) material characterization specimens.

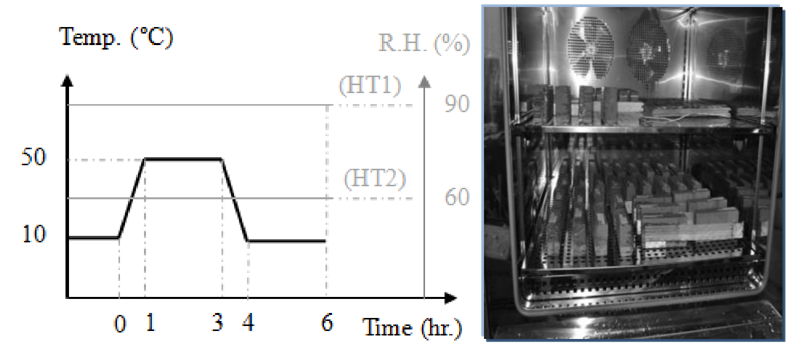

(a)

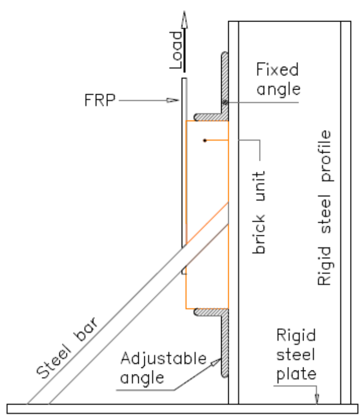

(b) (c)

Fig. 2. Test set-up: (a) Exposure cycles; (b) single-lap shear test setup; (c) tensile test setup.

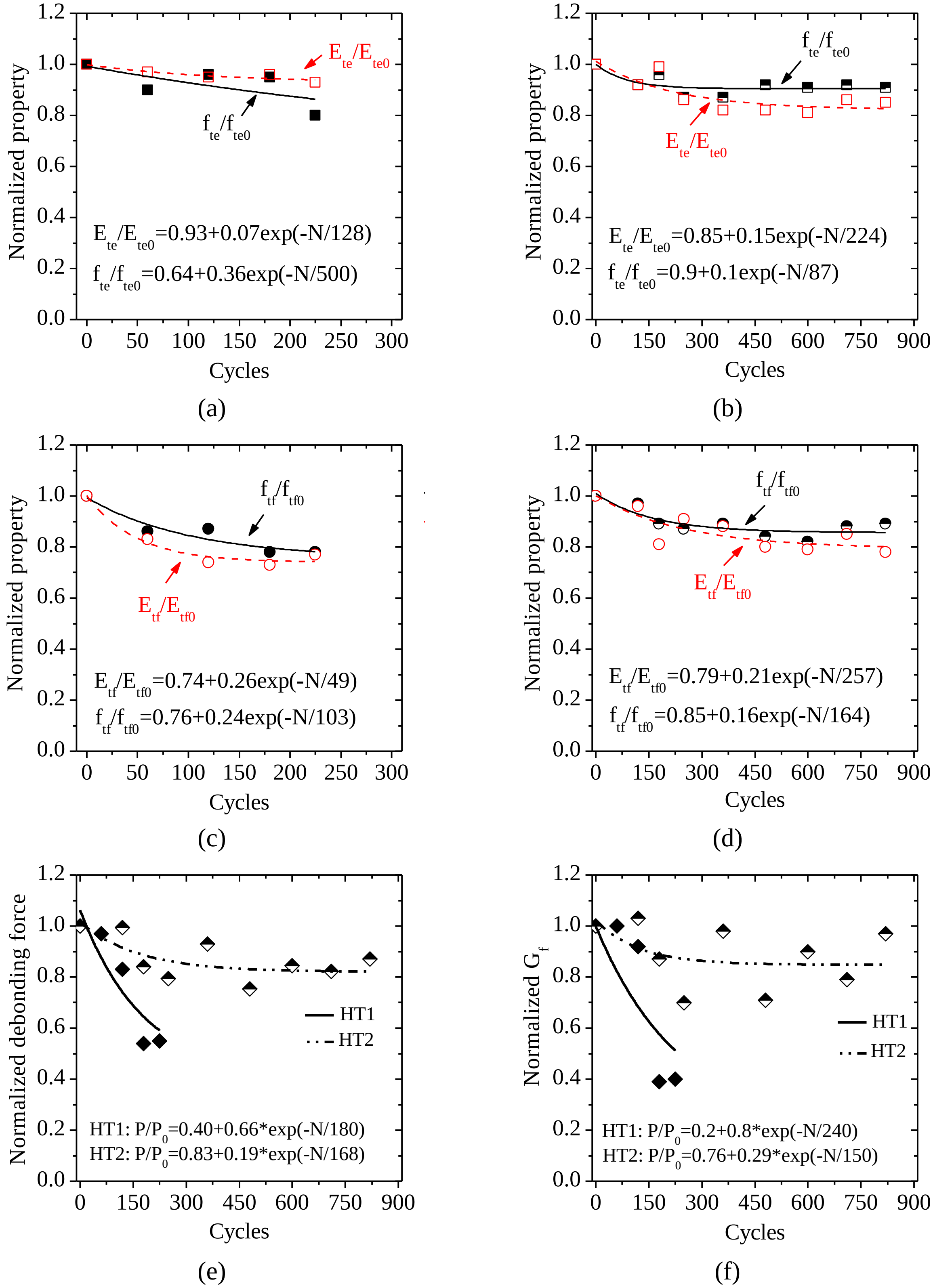

Fig. 3. Experimentally obtained hygrothermal degradation: (a) epoxy resin in HT1 environment; (b) epoxy resin in HT2 environment; (c) GFRP in HT1 environment; (d) GFRP in HT2 environment; (e) debonding force; (f) bond fracture energy.

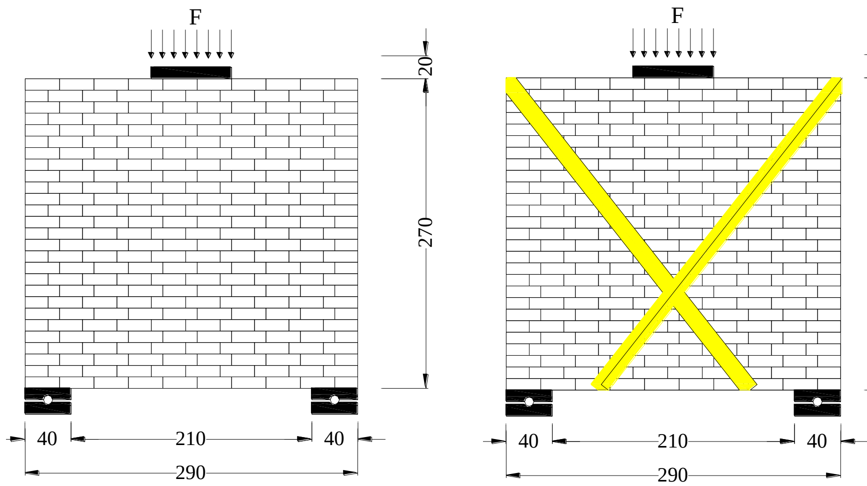

(a) (b)

Fig. 4. Panels selected for verification of the numerical model: (a) Pan A; (b) Pan C.

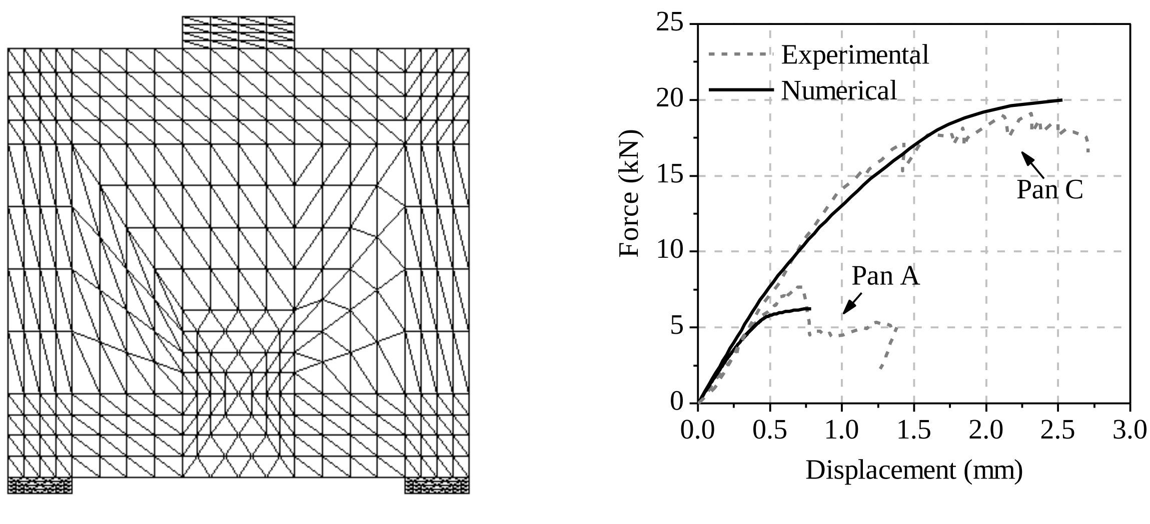

(a) (b)

Fig. 5. Finite element model: (a) adopted mesh for the reference walls; (b) comparison between numerical and experimental force-displacement curves.

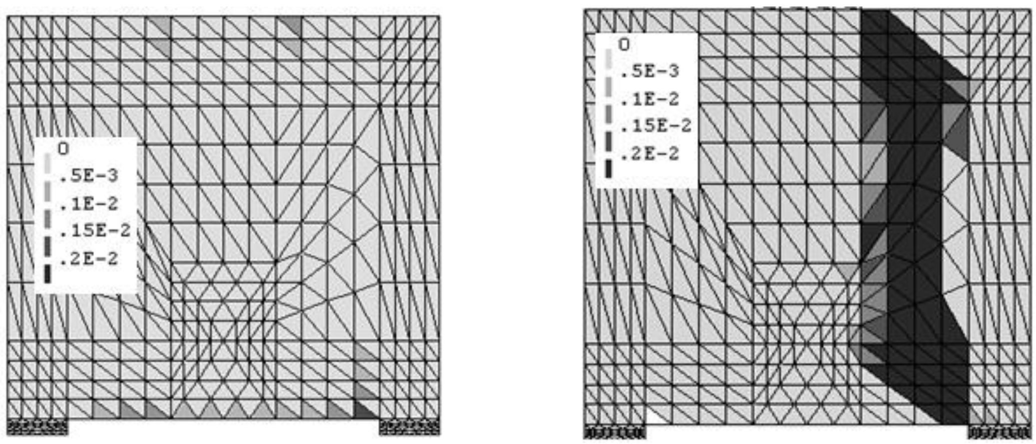

(a) (b)

Fig. 6. Tensile plastic strains in: (a) Pan A; (b) Pan C.

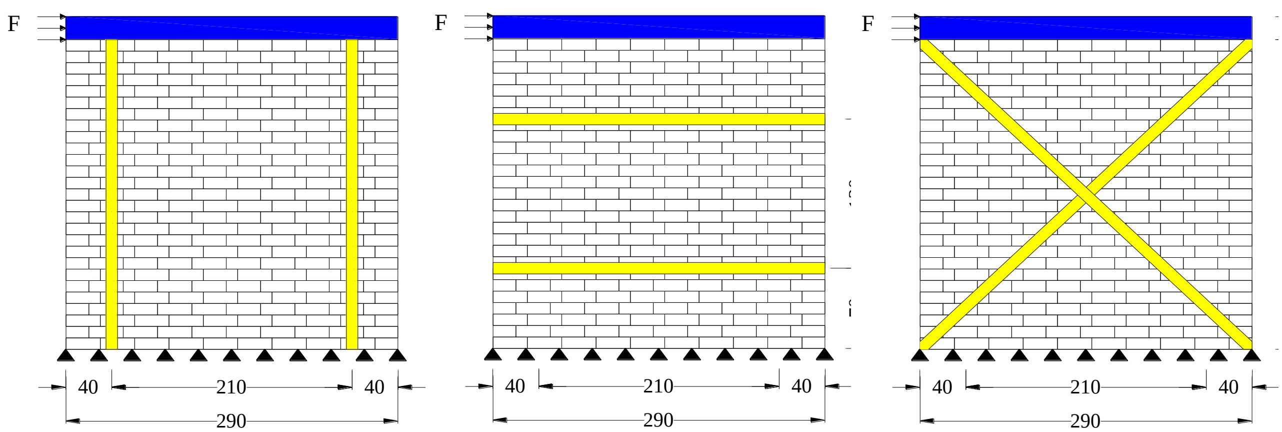

(a) (b) (c)

Fig. 7. Selected strengthening schemes: (a) scheme 1; (b) scheme 2; (c) scheme 3.

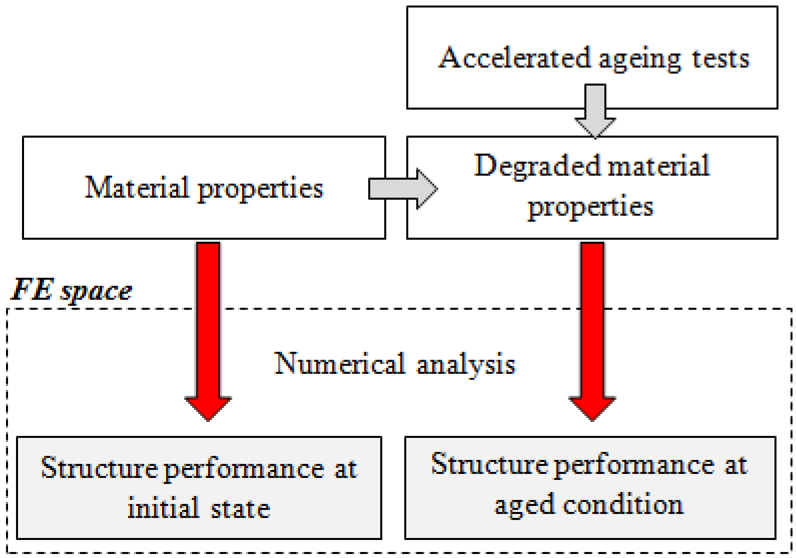

Fig. 8. Procedure followed for analysis of the walls.

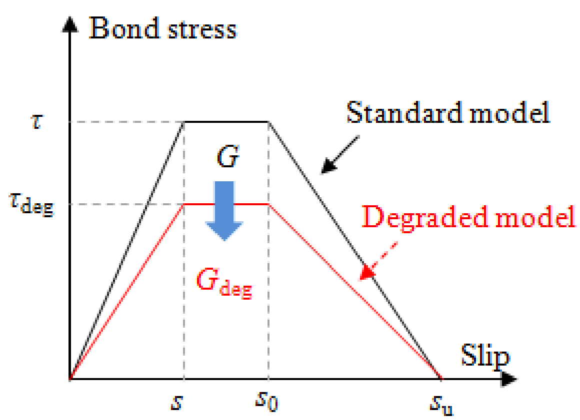

Fig. 9. Degradation model for the bond-slip law.

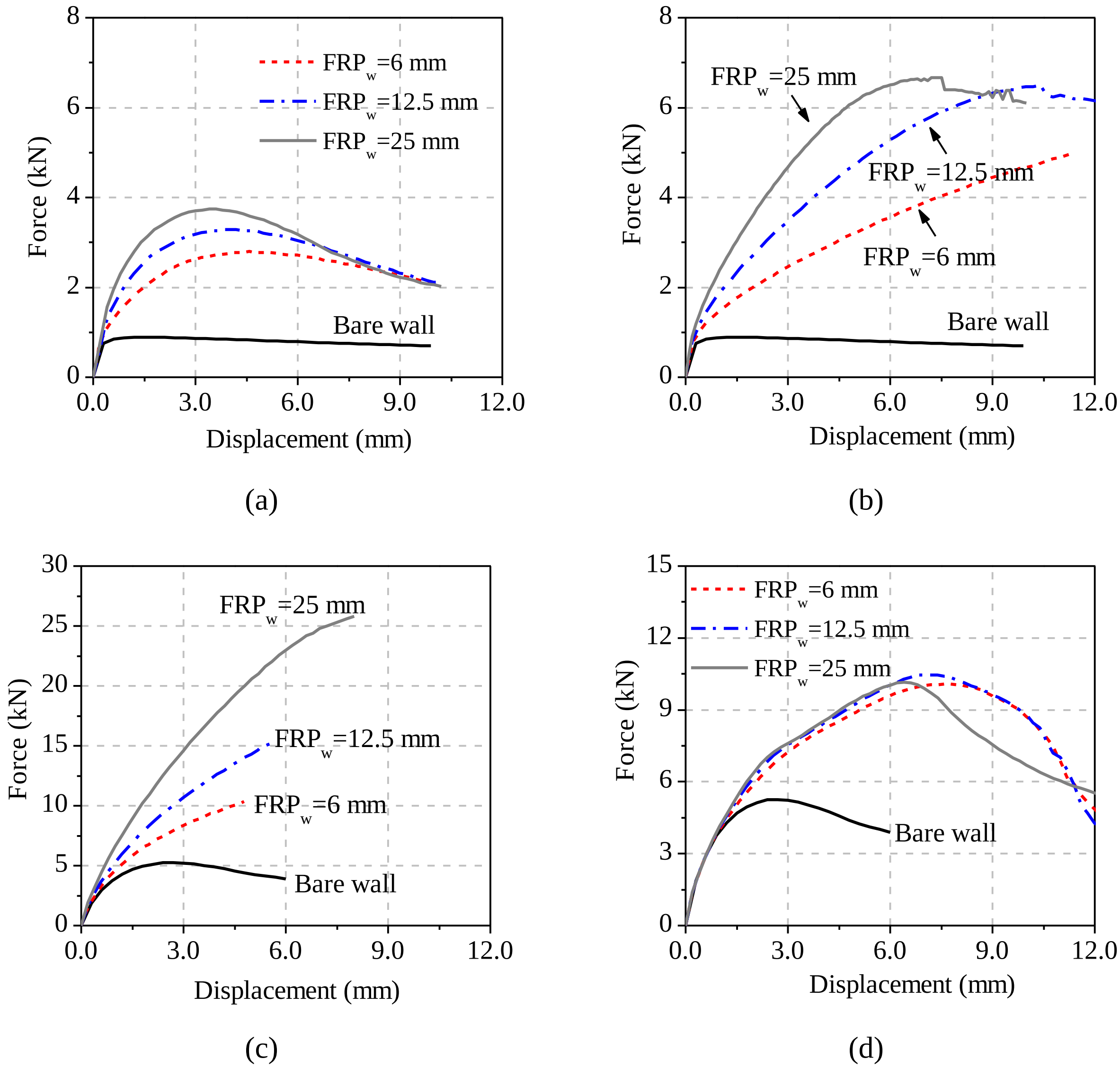

Fig. 10. Force-displacement behavior of selected hypothetical walls: (a) Wall 1; (b) Wall 2; (c) Wall 3; (d) Wall 4.

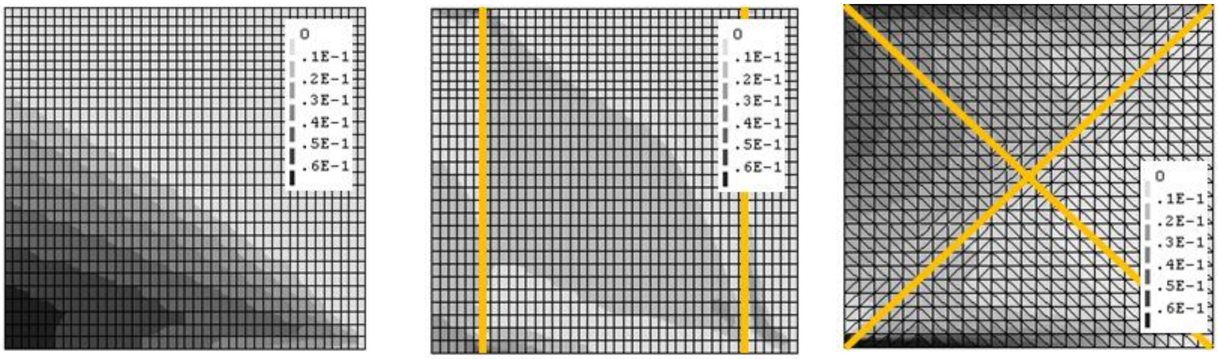

(a) (b) (c)

Fig. 11. Tensile plastic strain distribution: (a) Walls 1 and 2 before strengthening; (b) Wall 1 after strengthening with FRP_w=6 mm; (c) Wall 2 after strengthening with FRP_w=6 mm.

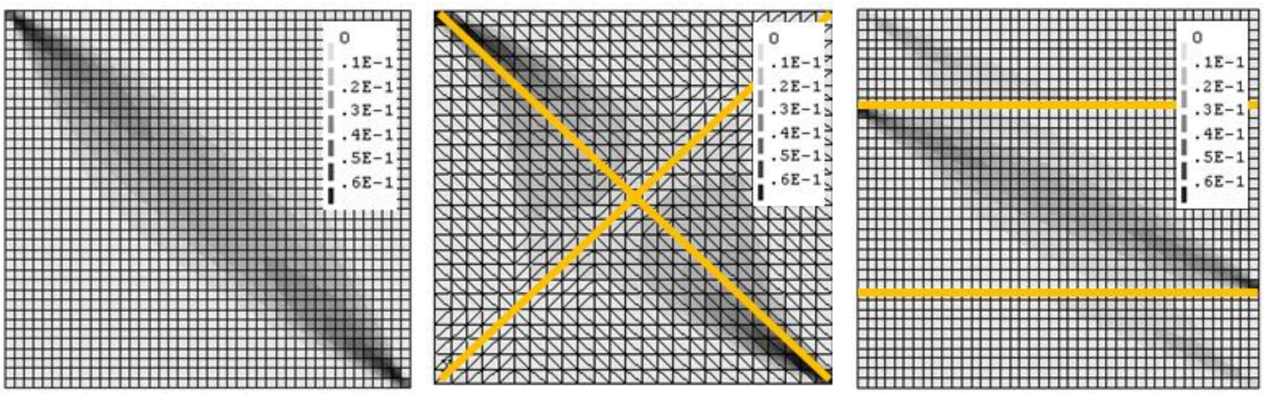

(a) (b) (c)

Fig. 12. Tensile plastic strain distribution: (a) Walls 3 and 4 before strengthening; (b) Wall 3 after strengthening with FRP_w=6 mm; (c) Wall 4 after strengthening with FRP_w=6 mm.

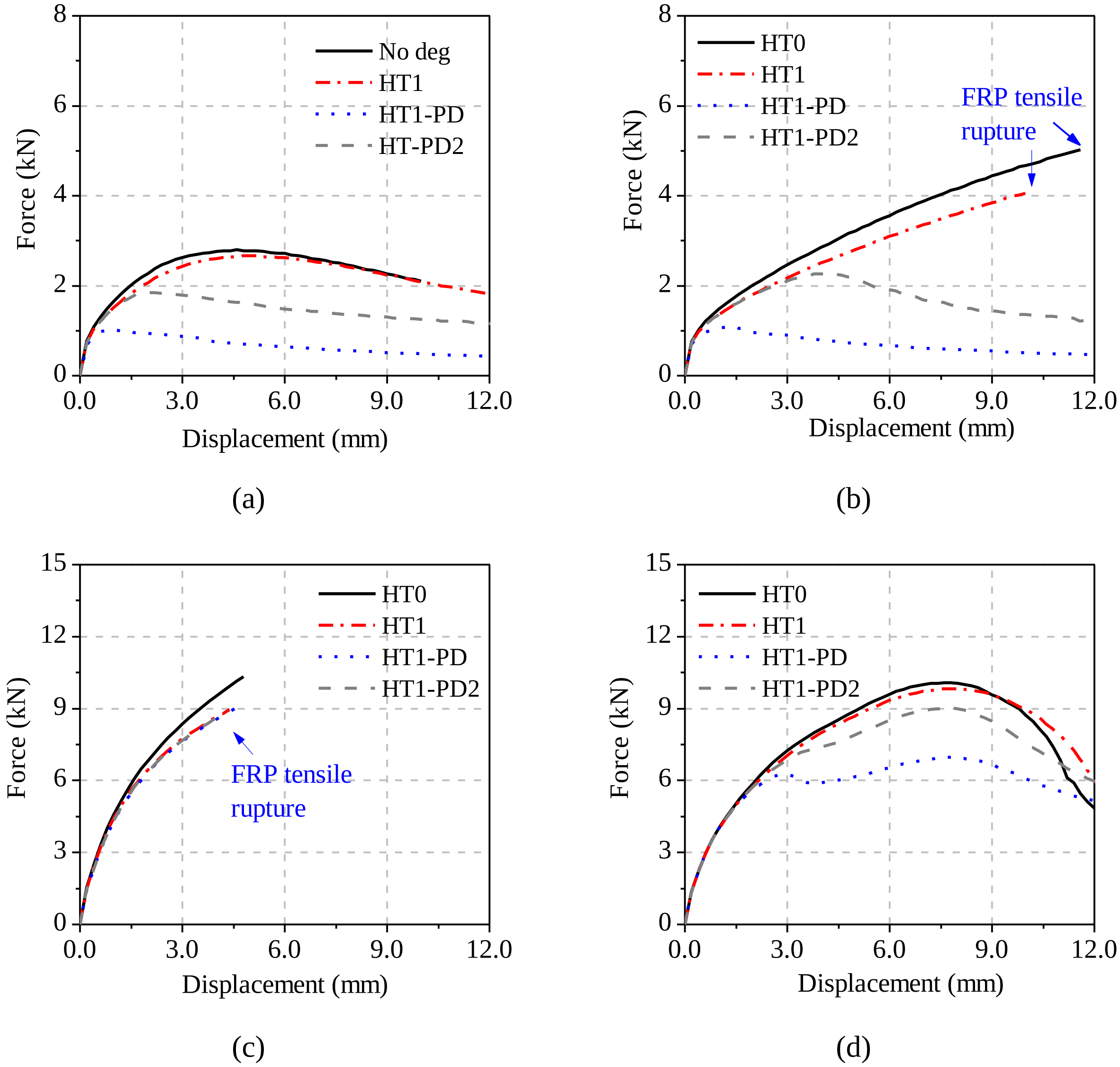

Fig. 13. Force-displacement behavior of selected hypothetical walls after ageing: (a) Wall 1; (b) Wall 2; (c) Wall 3; (d) Wall 4.

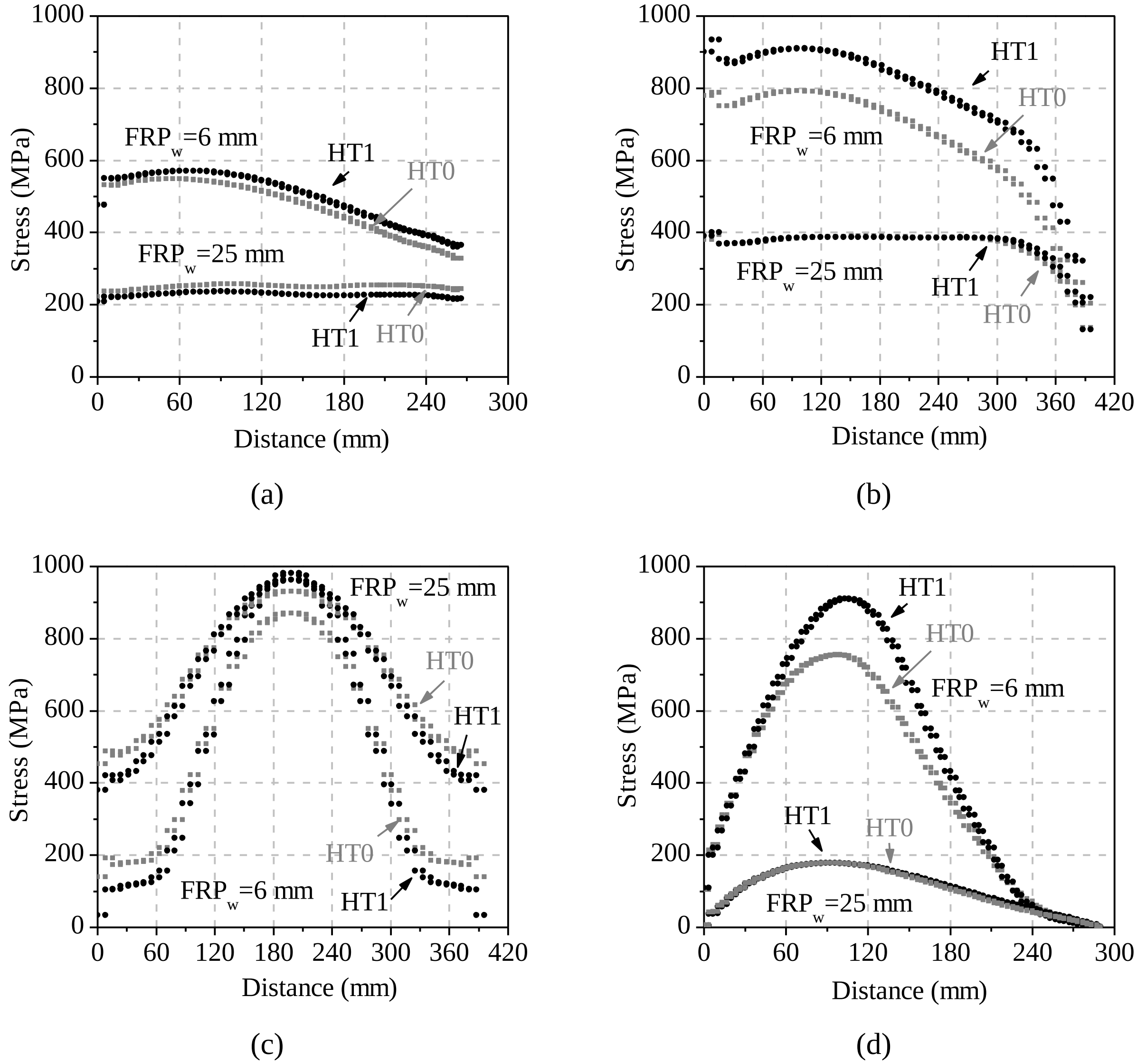

Fig. 14. FRP axial stress distribution at the peak load: (a) Wall 1; (b) Wall 2; (c) Wall 3; (d) Wall 4.

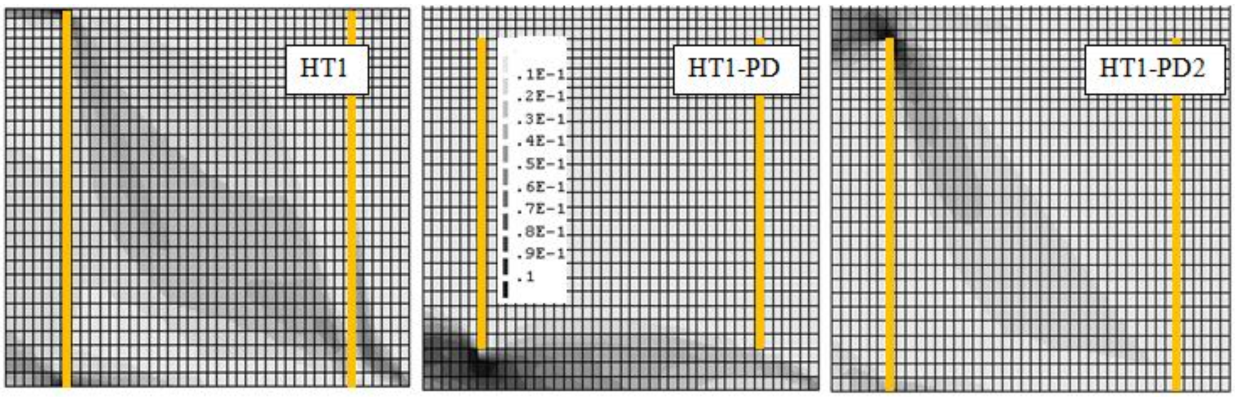

Fig. 15. Tensile plastic strain distribution on Wall 1 aged in different conditions.

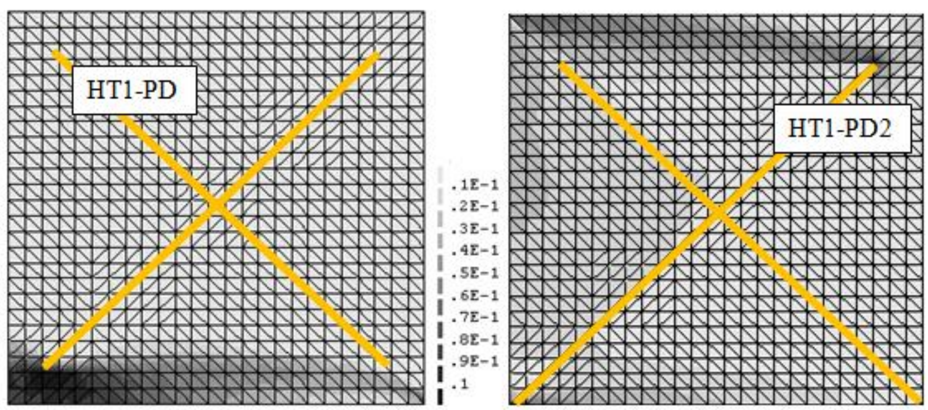

Fig. 16. Tensile plastic strain distribution on Wall 2 aged in different conditions.

Table 1. Masonry mechanical parameters.

Masonry mechanical parameters		
Elastic modulus along x-direction	E_{xx} (MPa)	1400
Elastic modulus along y-direction	E_{yy} (MPa)	1050
Poisson's ratio	ν_{xy}	0.18
Shear modulus	G_{xy} (MPa)	370
Tensile strength along x-direction	f_{tx} (MPa)	0.8
Tensile strength along y-direction	f_{ty} (MPa)	0.2
Compressive strength along x-direction	f_{cx} (MPa)	8.0
Compressive strength along y-direction	f_{cy} (MPa)	6.7
Fracture energy in tension along x-direction	G_{ftx} (N/mm)	0.02
Fracture energy in tension along y-direction	G_{fty} (N/mm)	0.02
Fracture energy in compression along x-direction	G_{fcx} (N/mm)	5.0
Fracture energy in compression along y-direction	G_{fcy} (N/mm)	10.0

Table 2. Bond-slip law parameters.

Exposure	τ_{max} (MPa)	S_0 (mm)	S_1 (mm)	S_u (mm)
No exposure	2	0.03	0.12	0.45

Table 3. Selected hypothetical walls.

Wall	Boundary	Strengthening	FRP width
W1	fixed-free	Scheme 1	6 mm 12.5 mm 25 mm
W2	fixed-free	Scheme 2	
W3	fixed-fixed	Scheme 2	
W4	fixed-fixed	Scheme 3	

Table 4. Material degradation after 225 cycles of all exposures.

Exposure	Bond properties		FRP properties			
	G_f		E_{tf}		f_{tf}	
	Reduction	Value (N/mm)	Reduction	Value (GPa)	Reduction	Value (MPa)
No ageing	0%	0.54	0%	80	0%	1250
HT1	-60%	0.22	-23%	62	-22%	975
HT2	-25%	0.41	-9%	73	-13%	1088

Table 5. Bond-slip parameters at 225 cycles of hygrothermal exposures.

Exposure	τ_{max} (MPa)	S_0 (mm)	S_1 (mm)	S_u (mm)
No ageing	2	0.03	0.15	0.45
HT1	0.8	0.03	0.15	0.45
HT2	1.5	0.03	0.15	0.45

Table 6. Changes in the strength and failure mode of Wall 1 and Wall 2 after ageing.

Wall	FRP width	Condition[1]	Pmax (kN)	Reduc. (%)	Failure mode[2]	Wall	FRP width	Condition[1]	Pmax (kN)	Reduc. (%)	Failure mode[2]
Wall 1	Bare wall	HT0	0.9	-	RO	Wall 2	Bare wall	HT0	0.9	-	RO
	6 mm	HT0	2.8	0.0	DT		6 mm	HT0	5.0	0.0	FRP TR
		HT1	2.7	5.0	DT			HT1	4.1	19.1	FRP TR
		HT1-PD	0.9	67.9	RO			HT1-PD	0.9	82.1	RO
		HT1-PD2	1.9	32.9	DT+RO			HT1-PD2	2.3	54.6	Sliding on top
		HT2	2.7	2.1	DT			HT2	5.0	0.0	FRP TR
	12.5 mm	HT0	3.3	0.0	DT		12.5 mm	HT0	6.5	0.0	TC
		HT1	3.1	4.9	DT			HT1	6.3	2.5	TC
		HT2	3.2	1.8	DT			HT2	6.5	0.6	TC
	25 mm	HT0	3.7	0.0	DT		25 mm	HT0	6.7	0.0	TC
		HT1	3.6	4.3	DT			HT1	6.6	1.5	TC
		HT2	3.7	1.1	DT			HT2	6.6	0.3	TC

[1]HT0: no conditioning is considered. HT1-PD: material degradation and FRP delamination due to HT1 exposure is considered. FRP delamination is assumed to occur at both FRP ends. HT1-PD2: material degradation and FRP delamination due to HT1 exposure is considered. FRP delamination is assumed to occur only at top end of FRP.

[2]RO: rocking; DT: masonry diagonal tension cracking; FRP TR: FRP tensile rupture; TC: masonry toe compression.

Table 7. Changes in the strength and failure mode of Wall 3 and Wall 4 after ageing.

Wall	FRP width	Condition[1]	Pmax (kN)	Reduc. (%)	Failure mode[2]	Wall	FRP width	Condition[1]	Pmax (kN)	Reduc. (%)	Failure mode[2]
Wall 3	Bare wall	HT0	5.1	-	DT	Wall 4	Bare wall	HT0	5.1	-	RO
	6 mm	HT0	10.3	0.0	FRP TR		6 mm	HT0	10.1	0.0	DT
		HT1	9.0	13.2	FRP TR			HT1	9.8	2.6	DT
		HT1-PD	9.0	13.0	FRP TR			HT1-PD	7.0	30.8	DT
		HT1-PD2	8.9	13.5	FRP TR			HT1-PD2	9.0	10.3	DT
		HT2	9.4	8.9	FRP TR			HT2	10.0	0.8	DT
	12.5 mm	HT0	15.3	0.0	FRP TR		12.5 mm	HT0	10.5	0.0	DT
		HT1	13.4	11.9	FRP TR			HT1	10.4	1.0	DT
		HT2	13.8	9.7	FRP TR			HT2	10.5	0.0	DT
	25 mm	HT0	25.8	0.0	FRP TR		25 mm	HT0	10.1	0.0	DT
		HT1	21.4	17.1	FRP TR			HT1	10.1	0.0	DT
		HT2	22.6	12.4	FRP TR			HT2	10.1	0.0	DT

[1]HT0: no conditioning is considered. HT1-PD: material degradation and FRP delamination due to HT1 exposure is considered. FRP delamination is assumed to occur at both FRP ends. HT1-PD2: material degradation and FRP delamination due to HT1 exposure is considered. FRP delamination is assumed to occur only at top end of FRP.

[2]RO: rocking; DT: masonry diagonal tension cracking; FRP TR: FRP tensile rupture; TC: masonry toe compression.